The transcription factor NR4A3 controls CD103+ dendritic cell migration

Kiwon Park,[1] Zbigniew Mikulski,[1] Goo-Young Seo,[2] Aleksander Y. Andreyev,[3] Paola Marcovecchio,[1] Amy Blatchley,[1] Mitchell Kronenberg,[2,4] and Catherine C. Hedrick[1]

[1]Division of Inflammation Biology and [2]Division of Developmental Immunology, La Jolla Institute for Allergy and Immunology, La Jolla, California, USA. [3]Department of Pharmacology and [4]Division of Biological Sciences, UCSD, La Jolla, California, USA.

The transcription factor NR4A3 (also known as NOR-1) is a member of the *Nr4a* family of nuclear receptors and is expressed in myeloid and lymphoid cells. Here, we have shown that *Nr4a3* is essential for the migration of CD103+ dendritic cells (DCs) to lymph nodes (LNs). *Nr4a3*-deficient mice had very few CD103+ migratory DCs (mDCs) present in LNs, and mixed-chimera studies revealed that this migratory defect was cell intrinsic. We further found that CD103+ DCs from *Nr4a3*-deficient mice displayed a marked loss of surface expression of the chemokine CCR7. This defect in CCR7 expression was confined to CD103+ DCs, as CCR7 expression on T lymphocytes was unaffected. Moreover, CCR7 was not induced on CD103+ DCs from *Nr4a3*-deficient mice in response to either administration of the TLR7 agonist R848 or infection with *Citrobacter rodentium* in vivo. The transcription factor FOXO1 has been shown to regulate CCR7 expression. We found that FOXO1 protein was reduced in *Nr4a3*-deficient DCs through an AKT-dependent mechanism. Further, we found a requirement for NR4A3 in the maintenance of homeostatic mitochondrial function in CD103+ DCs, although this is likely independent of the NR4A3/FOXO1/CCR7 axis in the regulation of DC migration. Thus, NR4A3 plays an important role in the regulation of CD103+ mDCs by regulating CCR7-dependent cell migration.

Introduction

The intestine has a mucosal surface that directly interacts with large quantities of food antigens and microorganisms daily. As a consequence, the gut is the accessible entry site for many pathogens. Because most food antigens and microorganisms are not harmful to the host, the immune system must be able to distinguish invading pathogens from innocuous antigens. Also, tolerance to those innocuous antigens is crucial to maintaining the fine balance between immunity and tolerance. If this balance is skewed, inflammatory diseases such as inflammatory bowel disease (IBD) and food allergies can ensue. Dendritic cells (DCs) play important roles in initiating adaptive immunity against pathogens as well as inducing tolerance against unharmful antigens and commensal microorganisms required to maintain this homeostasis.

In homeostatic conditions, CD103+ migratory lamina propria DCs (LPDCs), including CD103+CD11b– and CD103+CD11b+ DCs, sample antigens from the gut lumen and from apoptotic epithelial cells, then migrate to mesenteric lymph nodes (MLNs) (1, 2) to promote antigen-specific T cell activation, including activation of FOXP3+ Tregs (3). LPDCs include at least 3 subsets: CD103+CD11b– DCs, which are derived from conventional DCs (cDCs), CD103–CD11b+ DCs, which are derived from monocytes (4), and CD103+CD11b+ DCs, which are of heterogeneous origin (5). CD103+CD11b– DCs promote FOXP3+ Tregs (6). CD103+CD11b+ DCs are known to activate protective Th17 responses in a *Citrobacter rodentium*–induced colitis model (5, 7).

Migration of CD103+CD11b– and CD103+CD11b+ DCs to MLNs largely relies on expression of the chemokine receptor CCR7. Several transcription factors are known to regulate CCR7 expression directly, including RUNX3 (8), FOXO1 (9, 10), NF-κB, and AP1 (11). The regulation of CCR7 by LXR-α has been controversial, as Bruckner et al. showed CCR7 downregulation by LXR-α, and Feig el al. showed CCR7 upregulation by an LXR-α agonist (12, 13). However, this discrepancy was reconciled by the finding that the serine 198 phosphorylation status of LXR-α regulates *CCR7* promoter activity (14). CCR7 expression can also be regulated by cytokines and lipid mediators in the tissue, including prostaglandin E2 (PGE2) (15, 16), thymic stromal lymphopoietin (TSLP) (17), and IFN-β (18).

Nr4a nuclear receptor family members include NR4A1, NR4A2, and NR4A3. These nuclear receptors function as transcription factors and are involved in various cellular processes including cell development and immune function. *Nr4a* family members can be induced by diverse stimuli including inflammatory cytokines, lipid mediators, calcium, and hormones in various tissues and cells including neurons, endothelial cells, adipocytes, muscles, macrophages, and T cells (19). *Nr4a3* has been shown to play an important role in cell survival and proliferation in nonhematopoietic cells (20, 21). *Nr4a3* expression in monocytes is probably antiatherogenic (22). In lymphocytes, *Nr4a3* is involved in the negative selection of T cells, together with *Nr4a1* (23). NR4A3 is expressed in macrophages (24, 25), but little is known about the role of *Nr4a3* in DCs. Studies have shown that NR4A3 is expressed in BM-derived DCs (BMDCs)(26) and is induced by TLR stimulation in vitro (27). Recently, Grajales-Reyes et al. showed that CD24+ and CD172a+ cDCs from mice express high levels of *Nr4a3* compared with their precursor cells pre-CD8 DCs
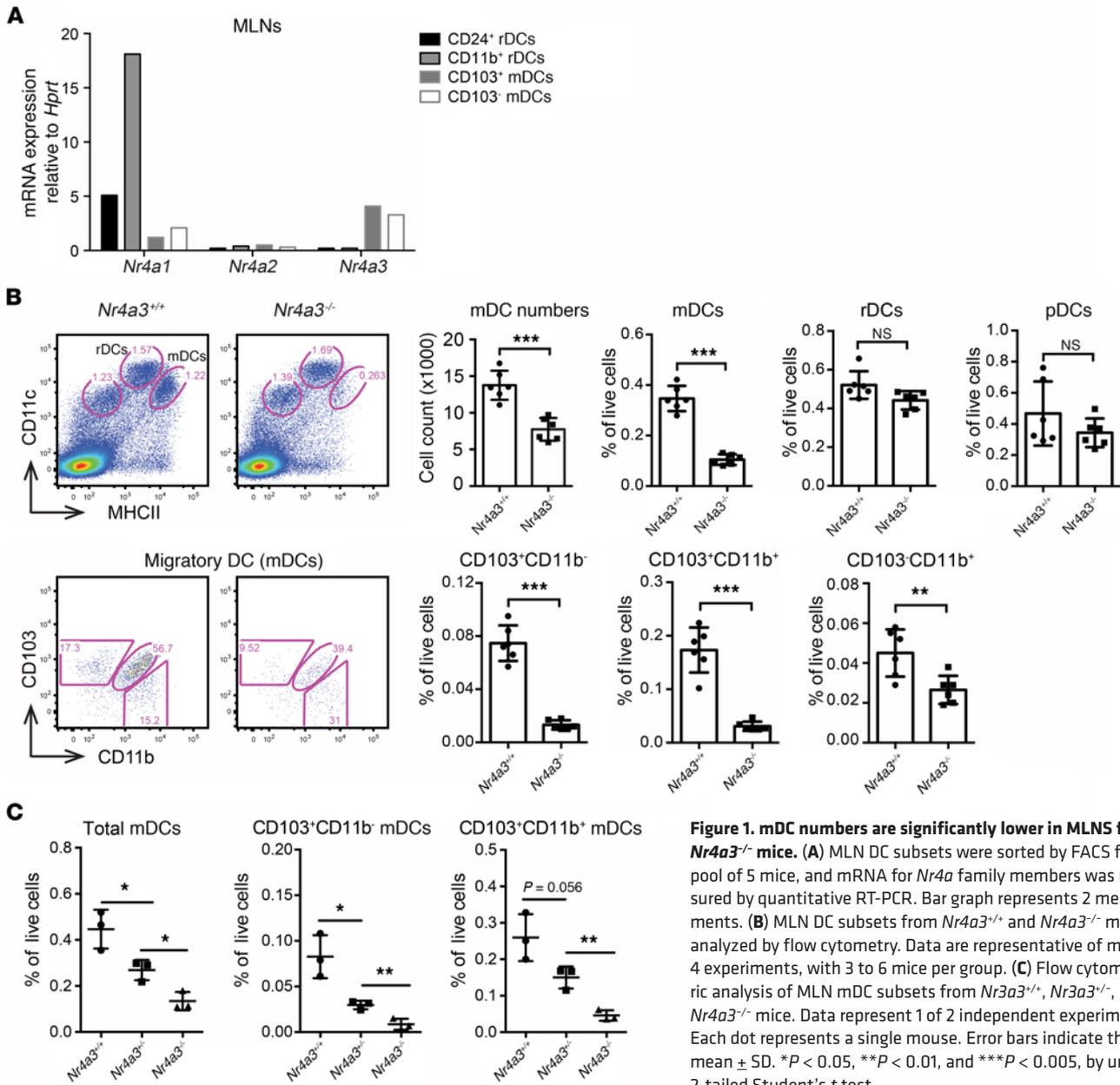
Figure 1. mDC numbers are significantly lower in MLNS from *Nr4a3*−/− mice. (**A**) MLN DC subsets were sorted by FACS from a pool of 5 mice, and mRNA for *Nr4a* family members was measured by quantitative RT-PCR. Bar graph represents 2 measurements. (**B**) MLN DC subsets from *Nr4a3*+/+ and *Nr4a3*−/− mice were analyzed by flow cytometry. Data are representative of more than 4 experiments, with 3 to 6 mice per group. (**C**) Flow cytometric analysis of MLN mDC subsets from *Nr3a3*+/+, *Nr3a3*+/−, and *Nr4a3*−/− mice. Data represent 1 of 2 independent experiments. Each dot represents a single mouse. Error bars indicate the mean ± SD. *P < 0.05, **P < 0.01, and ***P < 0.005, by unpaired, 2-tailed Student's *t* test.

and pre-CD4 DCs, respectively (28). However, a specific function for NR4A3 in DCs in vivo has not been defined. Therefore, in the present study, we investigated a role for *Nr4a3* in DC function and determined that this transcription factor is essential for the migration of a subset of intestinal DCs.

Results

Nr4a3 is highly expressed in migratory DCs in MLNs. To investigate a possible role for *Nr4a* family members in DC development and function, we analyzed lymphoid DC populations in C57BL/6J mice by flow cytometry. LN-resident DCs were divided into 3 subsets on the basis of CD4 and CD8 expression (29). Because CD8α+ rDCs are all CD24+, CD24+CD11b− DCs represent CD8α+ DCs, and CD24−CD11b+ DCs include CD4+ and CD4−CD8− DCs. Migratory DC (mDC) populations were gated using CD103 and CD11b. Detailed gating strategies for the flow cytometric analyses

in this study are described in the Supplemental materials (Supplemental Figures 2–4; supplemental material available online with this article; doi:10.1172/JCI87081DS1). Unlike skin-draining LNs (SLNs), which contain only 2 mDC subsets of CD103+CD11b− DCs and CD103−CD11b+ DCs (30, 31), MLNs contain 3 subsets of mDC populations: CD103+CD11b−, CD103+CD11b+, and CD103−CD11b+ DCs (4). Given the low numbers of CD103+ DCs in MLNs, CD103+CD11b− and CD103+CD11b+ DCs were pooled together (Supplemental Figure 1A). We measured mRNA expression of *Nr4a* family members in CD24+CD11b− and CD24−CD11b+ LN-resident DCs (rDCs) and CD103+ and CD103− mDCs. Interestingly, both mDC populations expressed high levels of *Nr4a3* mRNA (Figure 1A). *Nr4a2* expression was extremely low in all DC populations tested. As NR4A1 and NR4A3 are also expressed in T cells, we compared NR4A1 and NR4A3 expression levels between MLN DC subsets and splenic CD4+ and CD8+ T cells. Although
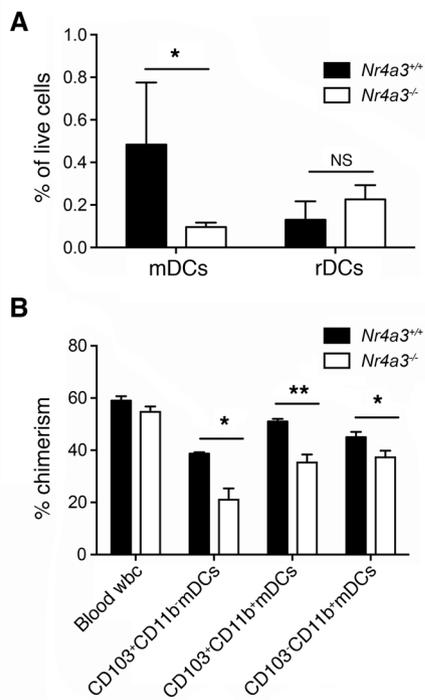
Figure 2. mDC defect in *Nr4a3*-deficient mice is hematopoiesis derived and cell intrinsic. (**A**) BM transplantation. BM from CD45.2 *Nr4a3*^{+/+} or CD45.2 *Nr4a3*^{−/−} mice was transplanted into sublethally irradiated CD45.1 recipient mice. After 8 weeks of reconstitution, mDCs and MLN-resident DCs (rDCs) were analyzed by flow cytometry. Results represent 1 of 2 independent experiments (*n* = 4 mice per group). (**B**) Mixed BM chimeras. BM hematopoietic stem cell progenitor cells from CD45.2 *Nr4a3*^{+/+} or CD45.2 *Nr4a3*^{−/−} mice were mixed 1:1 with CD45.1 cells to make CD45.2 *Nr4a3*^{+/+} plus CD45.1 and CD45.2 *Nr4a3*^{+/+} plus CD45.1 chimeras. 1:1 BM precursor mixtures were transferred into sublethally irradiated CD45.1/2 heterozygous mice. After 10 days, the mice were sacrificed for analysis. DC populations were analyzed in colon and MLNs. BM reconstitution was assessed in blood samples. The percentage of CD45.2 cells was calculated from total donor cells that included CD45.2 and CD45.1 cells. Results represent 1 of 2 independent experiments (*n* = 3–4 mice per group). *$P < 0.05$ and ** $P < 0.01$, by an unpaired 2-tailed Student's *t* test.

both CD4^{+} T cells and CD8^{+} T cells expressed NR4A1 and NR4A3, the expression levels of NR4A3 were much higher in the MLN DC subsets (Supplemental Figure 1B), suggesting that NR4A3 plays a specialized role in mDCs.

On the basis of these data, we examined the number and frequency of DC populations in *Nr4a1*^{−/−} and *Nr4a3*^{−/−} mice. Although *Nr4a1* expression in LN-resident DCs was quite high, we found no dramatic differences in the numbers of total LN-resident DC or mDC populations in *Nr4a1*^{−/−} mice (data not shown), so we did not explore this further.

However, we found that *Nr4a3*-deficient mice had significant reductions in mDC numbers (Figure 1B), as shown by the gating strategy described in Supplemental Figure 2. CD103^{+}CD11b^{−} and CD103^{+}CD11b^{+} subsets were significantly decreased, and CD103^{−}CD11b^{+} subsets were slightly lower in *Nr4a3*^{−/−} mice in terms of frequencies and cell numbers compared with WT mice. However, the number of total LN-resident DCs was not different, although we did detect a slight reduction in the CD8a^{+} DC subset numbers

(Supplemental Figure 5A). The specific reduction of mDCs in LNs was also found in skin-draining LN (SLN) as shown in Supplemental Figure 7A (gating strategy shown in Supplemental Figure 6), and in para-aortic LNs (data not shown). Thus, the loss of mDCs in lymphoid tissue in NR4A3-deficient mice appears to be systemic. We also examined splenic DC populations, since the spleen is a special lymphoid organ that lacks mDCs. We analyzed splenic DC subsets using the gating strategy shown in Supplemental Figure 3 and found no differences in these splenic DC subsets (Supplemental Figure 5B), confirming that the defect in *Nr4a3*^{−/−} mice is selective for mDC subsets.

NR4A3-deficient mDCs have impaired migration to LNs. mDCs in the gut move from the small intestine and colon to MLNs to present antigens, including self and nonself, from tissues to T cells. To address whether the lack of mDCs in *Nr4a3*^{−/−} MLNs is caused by changes in migration or is a developmental issue, we first quantified migratory LPDCs in small intestine and colon (Supplemental Figure 5, C and D), using the gating strategy described in Supplemental Figure 4. Unlike in LNs, high expression of CD11c and MHC II was not sufficient to identify the LPDC population, given the presence of CD11c^{+}MHC-II^{+} macrophages within the gut. To exclude macrophages from the LPDC population, CD64^{+} cells were excluded from LPDC gating (Supplemental Figure 4), because CD64 expression distinguishes macrophages from DCs (32, 33). Interestingly, no significant differences in small intestine or colon LPDC numbers or subsets were observed (Supplemental Figure 5, C and D). However, we found that langerin^{+}CD103^{+} and CD103^{−}CD11b^{+} dermal DC subsets were slightly increased in ear skin (Supplemental Figure 7B). We observed no differences in the numbers of lamina propria (LP) macrophages (data not shown). These data indicate that NR4A3-deficient LPDCs are present in tissues at normal levels, suggesting that *Nr4a3*^{−/−} mDCs may have an impaired ability to migrate to LNs.

To determine whether *Nr4a3* is a dominant driver of this defect, mDCs from MLNs of heterozygous *Nr4a3*^{+/−} mice were compared with DCs from WT *Nr4a3*^{+/+} and homozygous *Nr4a3*^{−/−} mice. We found a gene dose–dependent effect of *Nr4a3* on MLN total mDC and CD103^{+} DC subsets (Figure 1C), suggesting that changes in *Nr4a3* expression probably drive CD103^{+} DC migration to LNs.

Defective migration of Nr4a3^{−/−} DCs is cell intrinsic. Since DCs acquire antigens from peripheral tissue, they express the chemokine receptor CCR7 to home to LNs in response to the CCL19/21 gradient present along lymphatic vessels. We first assessed the expression levels of CCL21 in *Nr4a3*^{−/−} mice. Mouse CCL21 includes 2 variants at position 65: CCL21-Leu and CCL21-Ser. CCL21-Leu is expressed on the initial lymphatic vessels in the periphery, and CCL21-Ser is expressed on the terminal lymphatic vessels of LN subcapsules (34). We used confocal microscopy to measure RNA (data not shown) and protein expression of CCL21-Leu on lymphatic vessels in the terminal ileum and observed no differences in CCL21 expression in the lymphatic vessels of *Nr4a3*^{−/−} mice (Supplemental Figure 8).

Next, to determine whether the loss of mDCs in lymphoid tissue was hematopoiesis derived, we performed a series of BM transplantation studies, in which BM from CD45.2 WT *Nr4a3*^{+/+} or CD45.2 *Nr4a3*^{−/−} mice was transferred into irradiated recipient CD45.1 mice. After 8 weeks of reconstitution, we analyzed total
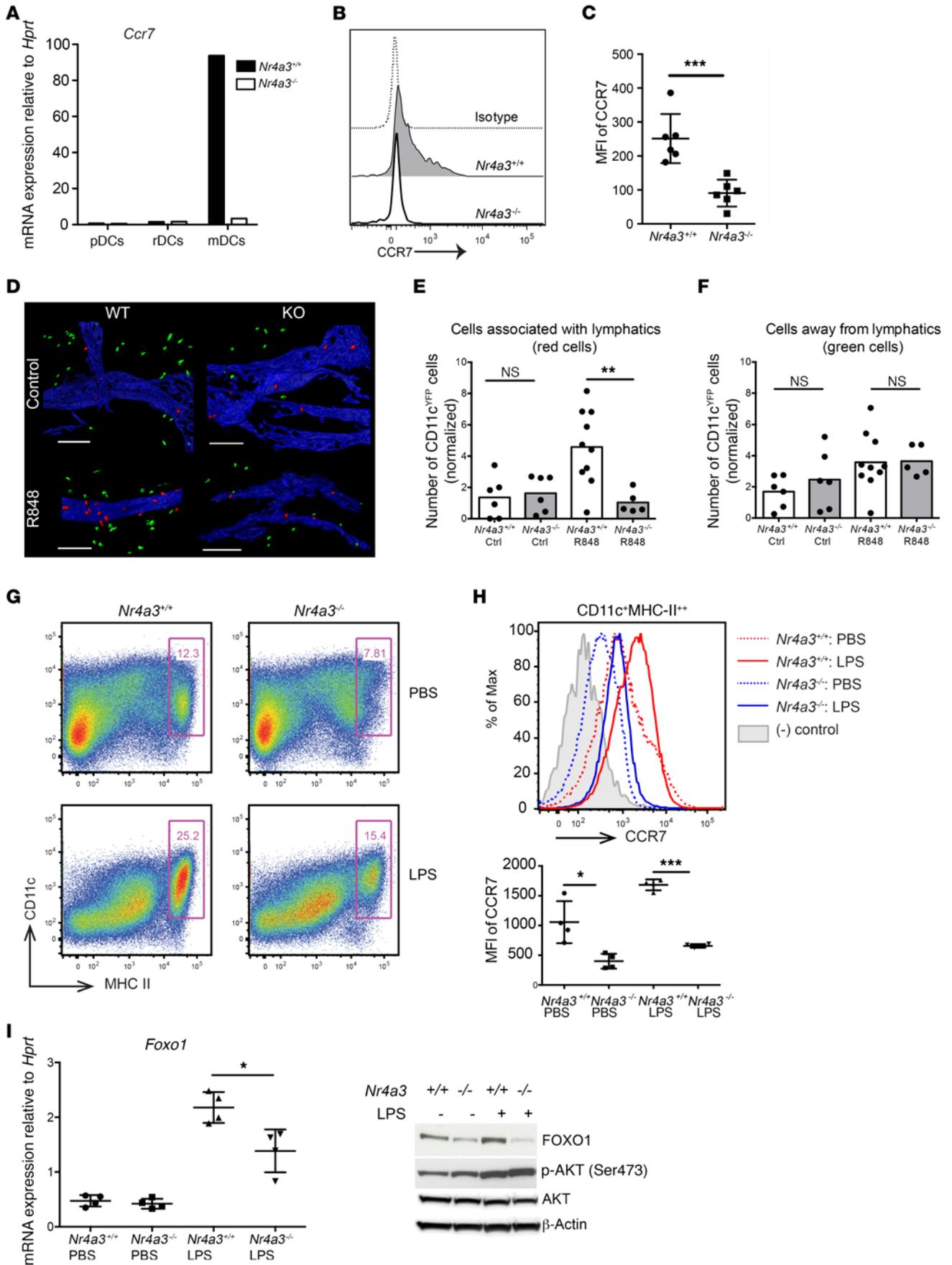
Figure 3. The migration defect of *Nr4a3$^{-/-}$* DCs is CCR7 dependent. (A) *Ccr7* mRNA expression. Plasmacytoid DCs (CD11c^{med}, MHC-II^{med}, PDCA-1$^+$, CD3$^-$, CD19$^-$), LN-resident DCs (CD11c$^+$, MHC-II^{med}, CD3$^-$, CD19$^-$), and mDCs (CD11c$^+$, MHC-II^{hi}, CD3$^-$, CD19$^-$) from WT and *Nr4a3$^{-/-}$* mice were sorted by FACS. Data represent pools of 5 mice per group. Results represent 1 of 2 independent experiments. **(B)** Histogram of CCR7 surface expression on mDCs. **(C)** MFI of CCR7 on mDCs (*n* = 6 mice per group). Results represent 1 of 3 independent experiments. **(D)** CD11c^{YFP} WT or CD11c^{YFP} *Nr4a3$^{-/-}$* mice were treated with R848 for 2 hours in vivo. Confocal whole-mount images of mesenteric lymphatic vessels from R848-treated CD11c^{YFP} WT or CD11c^{YFP} *Nr4a3$^{-/-}$* mice were analyzed using Imaris software. Lymphatics (blue) were isosurfaced, and distance transformation was applied to create a new channel that encoded the 3D distance from the lymphatic vessels. CD11c^{YFP} cells (green) were isosurfaced and classified as being associated with lymphatics (red) when the distance from the lymphatics was less than 15 μm. To normalize between the different data sets, the number of cells associated with lymphatics was divided by the volume of lymphatic vessels (expressed in μm^3 and divided by 100,000). **(E)** Numbers of YFP$^+$ cells associated with lymphatic vessels (red). **(F)** Numbers of YFP$^+$ cells away from lymphatic vessels (green). **(G)** Day-7 BMDCs were stimulated with 0.5 μg/ml LPS for 36 hours. CD11c$^+$MHC-II^{++} cells were gated for CCR7 expression. **(H)** MFI of CCR7 expression on CD11c$^+$MHC-II^{++} cells was analyzed by flow cytometry. Representative histogram (top) and dot plot of individual mouse samples (bottom). Max, maximum. **(I)** Expression of *Foxo1* mRNA and FOXO1, p-AKT, AKT, and β-actin proteins from CD11c$^+$ BMDCs, stimulated with or without LPS. Results from **G** and **I** represent 1 of 3 to 4 independent experiments. *$P < 0.05$, **$P < 0.01$, and ***$P < 0.001$, by unpaired, 2-tailed Student's *t* test.

mDCs and their subsets and found that mDCs were significantly reduced only in the mice that received NR4A3-deficient BM (Figure 2A), indicating that the defect was hematopoietic cell derived and suggesting that the defect in migration may be cell intrinsic. Next, we used a mixed-chimera approach, in which lineage-depleted hematopoietic stem cell progenitors were isolated from CD45.2 *Nr4a3$^{-/-}$* and CD45.1 mice, mixed at a 1:1 ratio, and transferred into sublethally irradiated CD45.1/2 heterozygous mice, as described in Methods. As a control, a 1:1 mixture of WT CD45.2 *Nr4a3$^{+/+}$* and CD45.1 hematopoietic stem cell progenitors was transferred into sublethally irradiated CD45.1/2 heterozygous mice. After 10 days of reconstitution, tissues were analyzed for mDC subsets. As shown in Figure 2B, there was an equal reconstitution of CD45.1 and CD45.2 cells in the blood. Moreover, progenitors from *Nr4a3$^{-/-}$* mice reconstituted mDCs to normal numbers in the colon but not in the MLNs, again indicating a defective migration of these cells from tissues to LNs (Figure 2B). As a positive control, normal numbers of resident DCs from *Nr4a3$^{-/-}$* mice repopulated the MLNs (Supplemental Figure 9), suggesting that the defect was selective for mDCs. We conclude from these data that there is a cell-intrinsic defect in CD103$^+$ mDCs in the absence of *Nr4a3* that impairs their migration from tissues to LNs.

Migration defect of Nr4a3$^{-/-}$ DCs is due to impaired CCR7 expression. We next explored mechanisms that would explain the defective migration of CD103$^+$ DCs in the absence of NR4A3, focusing on expression of CCR7 on mDCs. The migration of DCs from intestinal LP to MLNs is known to be CCR7 dependent (2). We measured the expression of *Ccr7* mRNA and surface CCR7 in total mDCs sorted from MLNs. Although mDCs in WT mice expressed abundant *Ccr7* mRNA, the few remaining mDCs in *Nr4a3$^{-/-}$* mice expressed almost no *Ccr7* mRNA (Figure 3A). Furthermore, CCR7 expression was markedly reduced on the surface of *Nr4a3$^{-/-}$* mDCs in MLNs (Figure 3, B and C). CD103$^+$CD11b$^-$ and CD103$^+$CD11b$^+$ subsets of mDCs from *Nr4a3$^{-/-}$* mice showed similar results (data not shown).

We next used CD11c^{YFP} mice that either expressed *Nr4a3* (WT) or had been crossed with *Nr4a3$^{-/-}$* mice (KO) to visualize mDCs in lymphatic vessels of the gut. Migrating CCR7$^+$ LPDCs attach to CCL21 to travel along the lymphatics. Since CCR7$^+$ DCs from LP are difficult to detect by flow cytometry and we also wished to visualize the mDCs within the lymphatic vessels, we used confocal microscopy. To stimulate migration, CD11c^{YFP} WT and CD11c^{YFP} *Nr4a3$^{-/-}$* mice were treated in vivo with the TLR7 agonist R848, and the mesentery lymphatic vessels (Figure 3D, blue) were

imaged 2 hours later. As shown in Figure 3, D and E, the number of YFP$^+$CD11c$^+$MHC-II$^+$ cells attached to lymphatic vessels (red cells) was significantly lower in mice lacking NR4A3. As a control, we found that the numbers of cells located away from lymphatic vessels (green cells) by more than 15 μm were not significantly different (Figure 3F). These results support the idea that the migration defect of *Nr4a3*-deficient mDCs is caused by reduced CCR7 expression, although they do not rule out an activation defect.

We also assessed CCR7 expression on *Nr4a3$^{-/-}$* DCs using a BMDC culture with granulocyte macrophage–CSF (GM-CSF) that mimicked monocyte-derived inflammatory DCs, because we observed that *Nr4a3* expression increased during the course of BMDC development with the addition of GM-CSF (data not shown). BMDCs cultured for 7 days in the presence of GM-CSF were stimulated with LPS for 36 hours to stimulate TLR4 signaling and were then analyzed for CCR7 and DC surface marker expression. First, we observed that the numbers of CD11c$^+$MHC-II^{++} cells from the *Nr4a3$^{-/-}$* cell culture were 40% lower than the numbers detected in WT cell culture. However, after LPS treatment, the fold increase in frequency was similar to that observed in WT cell culture, suggesting that the TLR-dependent DC activation pathway may be comparable to that in WT cells (Figure 3G). However, CCR7 expression on *Nr4a3$^{-/-}$* DCs was much lower than that on WT DCs, even at baseline (Figure 3H). Further, although LPS stimulation increased the number of CCR7$^+$ BMDCs in *Nr4a3$^{-/-}$* mice, the mean fluorescence intensity (MFI) of CCR7 as well as the frequency of CCR7$^+$ DCs were much lower than those in WT cells (Figure 3H).

To understand how *Nr4a3* regulates *Ccr7*, we first performed a series of promoter-reporter assays. We analyzed 3.3 kb of the mouse *Ccr7* promoter upstream from the transcriptional start site using MacVector software and found 2 NR4A-binding motifs (NBRE, monomer-binding motif) and 5 putative C/EBP α/β–binding motifs (Supplemental Figure 10A). We cloned this region into pGL4-luciferase and found no evidence for a direct regulation of *Ccr7* promoter activity by NR4A3 in vitro (Supplemental Figure 10B). C/EBP β was used as a positive control for regulating *Ccr7* promoter activity (15). We concluded that CCR7 expression must be regulated by NR4A3 through an indirect mechanism.

As FOXO1 has been shown to be a critical transcription factor for CCR7 expression in T cells (9) and DCs (10), we next measured *Foxo1* mRNA and protein expression using CD11c$^+$ BMDCs. As shown in Figure 3H, LPS drove the induction of CCR7 expression in DCs. *Foxo1* mRNA and protein expression levels were increased by LPS stimulation in WT *Nr4a3$^{+/+}$* cells (Figure 3I). *Foxo1* mRNA
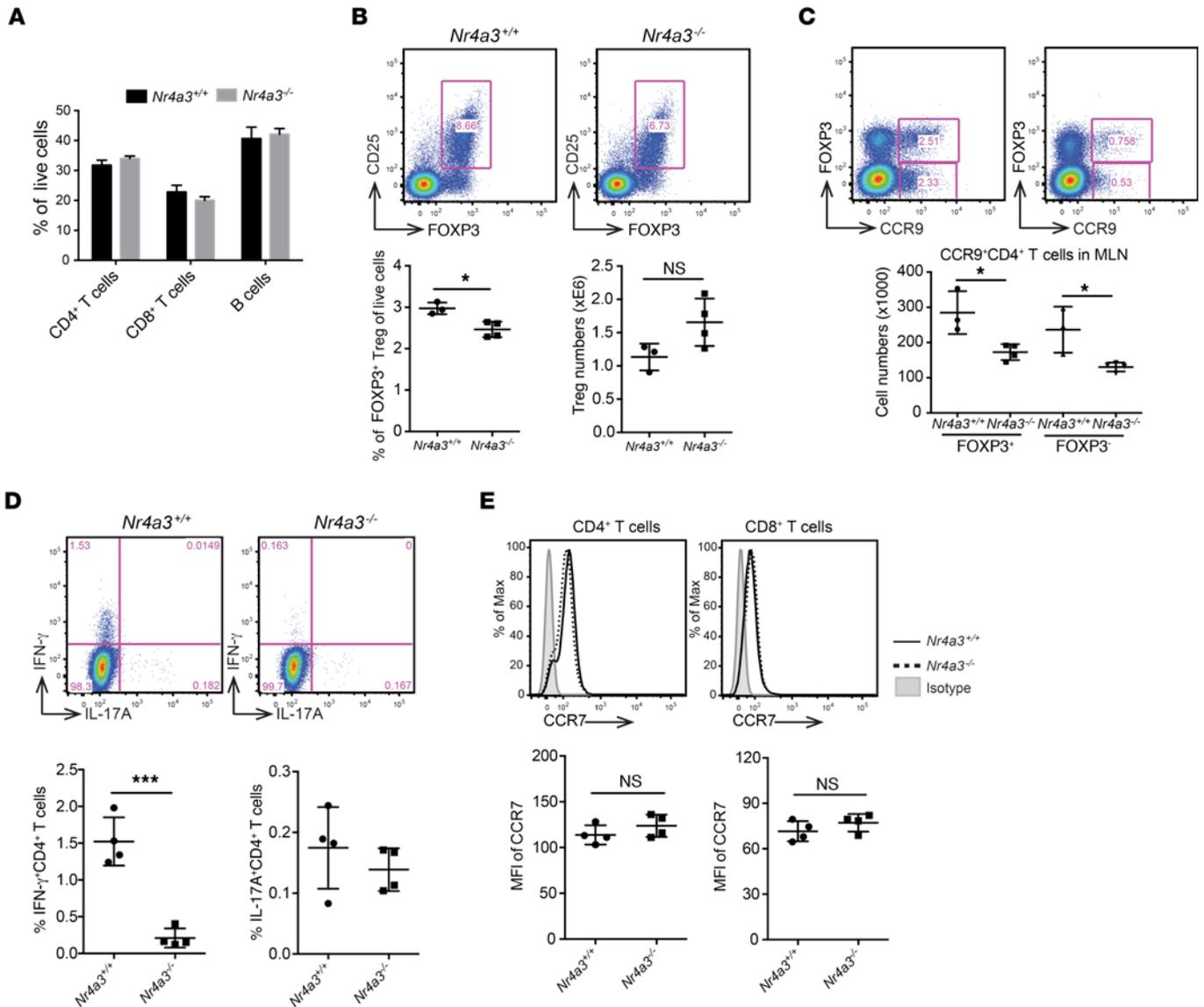
Figure 4. *Nr4a3* deficiency does not change lymphocyte composition or CCR7 expression on T cells but impairs steady-state T cell activation in MLNs. Percentages of T cells and B cells (**A**) and of CD4+CD25+FOXP3+ T cells (**B**) and CD4+CCR9+ T cells (**C**) were measured by flow cytometry. Steady-state IFN-γ+CD4+ T cells and IL-17A+CD4+ T cells were measured (**D**). Histogram showing CCR7 expression on CD4+ and CD8+ T cells and plot showing the MFI of CCR7 (**E**). Data represent 1 of 3 independent experiments. *P < 0.05 and ***P < 0.001, by unpaired, 2-tailed Student's t test.

was also slightly increased by LPS treatment of *Nr4a3−/−* DCs, but to a lesser extent (Figure 3I). This did not correlate with FOXO1 protein expression, which was lower in *Nr4a3−/−* mouse DCs, both at baseline and after treatment with LPS (Figure 3I). FOXO1 protein levels are primarily regulated through phosphorylation of the AKT pathway, which directs FOXO1 for polyubiquitination and degradation (35). We found increased AKT phosphorylation (at serine 473) in both unstimulated and LPS-stimulated *Nr4a3−/−* DCs (Figure 3I), suggesting that the observed reduction in FOXO1 protein was likely caused by AKT activation, which triggered FOXO1 degradation.

Migration defect of Nr4a3−/− DCs impairs T cell activation in MLNs. Retinoic acid plays an important role in MLN DCs to aid in the induction of FOXP3+ Tregs and to imprint activated T cells to migrate to gut tissue via CCR9 induction (36, 37). The key enzyme for these functions is retinaldehyde dehydrogenase 2

(RALDH2, encoded by *Aldh1a2*), which is highly expressed in LPDCs. First, we measured mRNA expression of *Aldh1a2*, encoding RALDH2, from flow cytometry–sorted total mDCs, LN-resident DCs, and plasmacytoid DCs (pDCs) from MLNs (Supplemental Figure 11A). Only WT mDCs expressed high levels of *Aldh1a2*. We found that *Nr4a3−/−* mDCs did not express *Aldh1a2*. We next measured RALDH enzyme activity by ALDE-FLUOR assay. LPDCs and migratory MLN mDCs from WT mice expressed high levels of RALDH. Although *Nr4a3−/−* LPDCs in the small intestine expressed RALDH, we found that *Nr4a3−/−* migratory MLN mDCs did not express RALDH. We also found that LP macrophages did not express RALDH (data not shown). Thus NR4A3-deficient CD103+ DCs express fully functional RALDH that potentially could allow them to induce iTregs and CCR9 expression, if they are able to successfully migrate to MLNs.
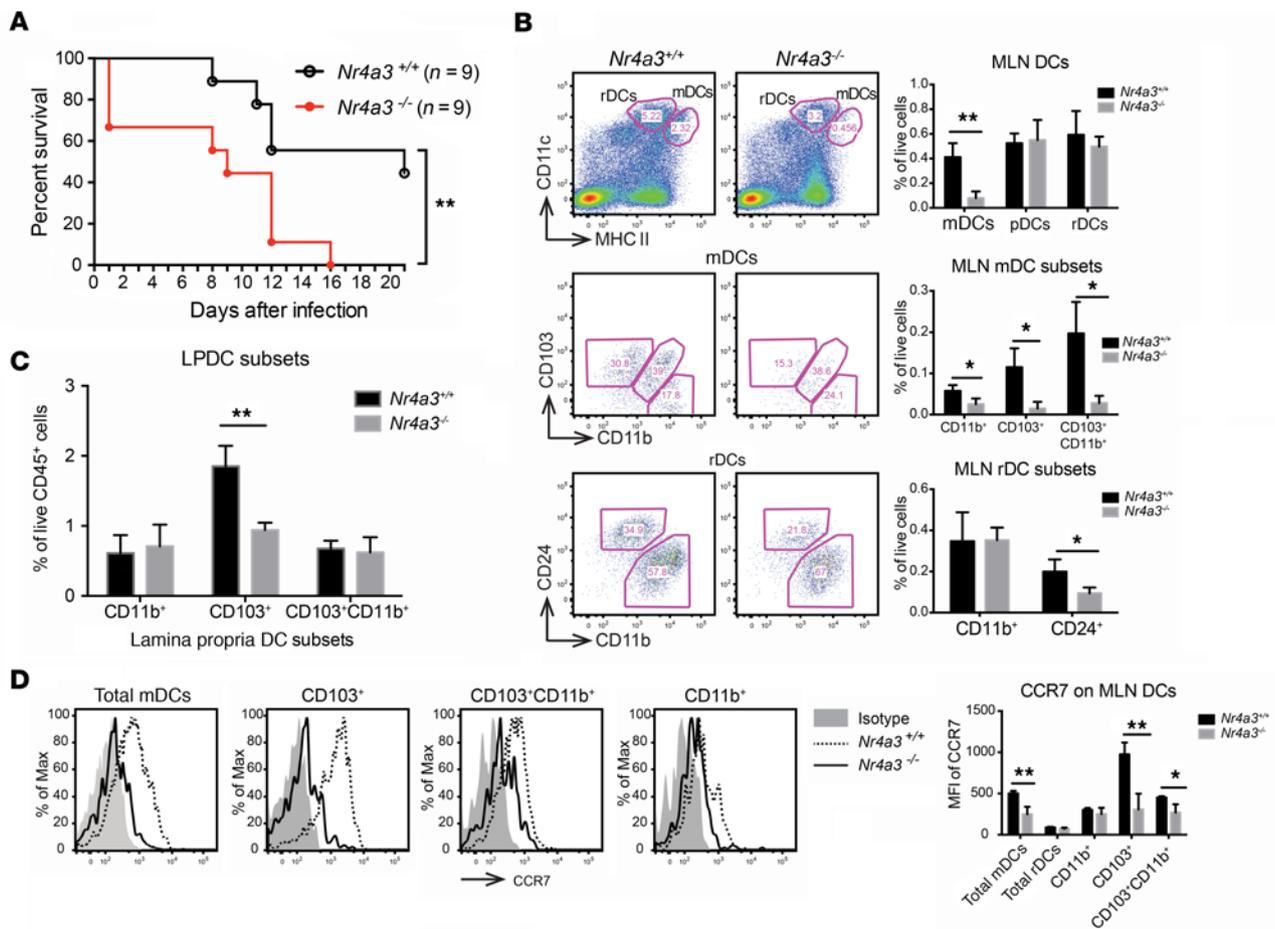
Figure 5. *Nr4a3⁻/⁻* mice are susceptible to *C. rodentium* infection, but CCR7 expression on mDCs is not increased. (**A**) *Nr4a3⁻/⁻* and *Nr4a3⁺/⁺* mice were infected with 1 × 10⁹ CFU *C. rodentium* by oral gavage. The appearance and survival of infected mice were monitored daily for 21 days.**P < 0.01, by log-rank (Mantel-Cox) test. Results represent 1 of 2 independent experiments (*n* = 9–10 mice per group). (**B–D**) MLN DC (**B**) and colon LPDC (**C**) subsets were analyzed by flow cytometry on day 8 after infection. The graphical summaries are representative of 4 mice per group. (**D**) Histograms plotting CCR7 expression of MLN DC subsets. A graphical summary of the MFI is shown. Results represent 1 of 2 independent experiments (*n* = 4 mice per group). *P < 0.05 and **P < 0.01, by unpaired, 2-tailed Student's *t* test.

We next examined whether Tregs and T effector cells in *Nr4a3⁻/⁻* mice are affected by the loss of CD103⁺ DCs in steady-state MLNs. We observed no differences in the composition of CD4⁺ T cells, CD8⁺ T cells, or B cells (Figure 4A). However, we detected reduced frequencies of FOXP3⁺ Tregs (Figure 4B) and CCR9⁺ T cells (Figure 4C) and significantly reduced frequencies of IFN-γ⁺CD4⁺ T cells (Figure 4D). We did not observe differences in IL-17A⁺CD4⁺ T cells (Figure 4D) in MLNs. As CCR7 is important for T cell homing to LNs, we assessed CCR7 expression on T cells and found that it was not affected by the absence of *Nr4a3* expression (Figure 4E). Thus, we conclude that the CCR7 defect observed in *Nr4a3⁻/⁻* mice is limited to mDCs and likely results in decreased percentages of CCR9⁺ T cells and IFN-γ⁺ T cells in MLNs.

CCR7 expression is not induced on CD103⁺ DCs in the absence of Nr4a3. We next asked whether *Nr4a3*-deficient mDCs could be mobilized to LNs by the induction of inflammatory cytokine pathways. Oral administration of the TLR7 agonist R848 has been shown to mobilize LPDCs to MLNs through pDC-mediated type 1 IFN and TNF-α production (38), which causes the induction of CCR7 on DCs (1). To determine whether R848 oral gavage could

mobilize CD103⁺ DCs, we treated mice with R848 and examined the mDC content in MLN DCs at 14 hours. Like *Nr4a3⁻/⁻* mice, *Ccr7⁻/⁻* mice have normal numbers and subsets of LPDCs in the gut, but deficient numbers of mDCs in MLNs (39). CD103⁺CD11b⁻ DC and CD103⁺CD11b⁺ mDC subsets from *Ccr7⁻/⁻* mice were dramatically reduced at steady state (Supplemental Figure 12A), indicating that these DCs utilize CCR7 for LN homing. However, CD103⁻CD11b⁺ DCs still migrated in the absence of CCR7 (Supplemental Figure 12A). We observed an increase in total mDC frequencies from all strains upon R848 treatment (Supplemental Figure 12B). Total numbers of mDCs from *Nr4a3⁻/⁻* mice were similar to those from *Ccr7⁻/⁻* mice (Supplemental Figure 12C). However, we did not observe an increase in CCR7 on mDCs from *Nr4a3⁻/⁻* mice in response to R848 (Supplemental Figure 12D).

Finally, we asked whether bacterial infection could induce CCR7 and LPDC migration in *Nr4a3⁻/⁻* mice by stimulating TLR-dependent CCR7 induction (40) in LPDCs. *Nr4a3⁻/⁻* mice were infected with *C. rodentium*, a murine model of *E. coli* infection in humans (41). *Nr4a3⁻/⁻* mice were more susceptible to *C. rodentium* infection than were WT mice (Figure 5A). Since most of the deaths occurred 8 days after infec-
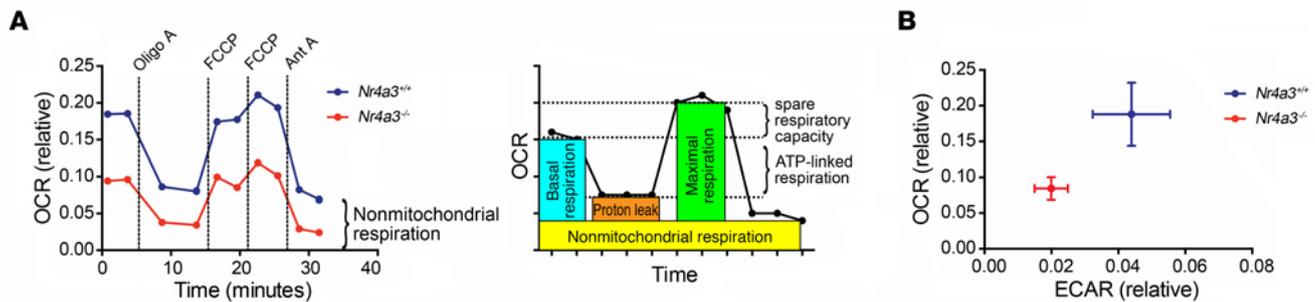
Figure 6. *Nr4a3* regulates mitochondrial function in BMDCs. (A) CD11c⁺ BMDCs were plated onto a XF96 plate, and OCRs and ECARs were measured with sequential treatment of oligomycin A (Oligo), FCCP, and antimycin A (Ant A) using a SeaHorse XFe 96 analyzer. After analysis, the cell numbers were measured by Hoechst 33342 staining for normalization of the ECARs and OCRs. The mean value of the relative OCRs is shown. A diagram of the OCR plot is shown. **(B)** Relative OCRs and ECARs are shown. $P < 0.0001$, by 2-way ANOVA for genotype, treatment, and interaction. Results represent 1 of 3 independent experiments. Each data point represents 5 technical replicates.

tion, we asked whether the adaptive immune response in *Nr4a3*⁻/⁻ mice was unable to control the infection. We analyzed CD4⁺ T cells from MLNs and colon on day 8 after infection. In MLNs, IFN-γ⁺ Th1 and IL-17A⁺ Th17 cell numbers were significantly lower in *Nr4a3*⁻/⁻ mice (Supplemental Figure 13). However, these differences were not observed in the colon (Supplemental Figure 13). Similar to what we observed at steady state, the number of MLN DCs from *Nr4a3*⁻/⁻ mice after infection was significantly lower than that of MLN DCs from WT mice (Figure 5B). However, CD103⁺CD11b⁻ LPDC numbers from *Nr4a3*⁻/⁻ mice were slightly decreased (Figure 5C), unlike in the steady state, in which no differences were observed between WT and *Nr4a3*⁻/⁻ mice. Moreover, *C. rodentium* infection did not cause an increase in the surface expression of CCR7 on *Nr4a3*⁻/⁻ mDCs (Figure 5D). These data collectively suggest that CCR7 expression is markedly reduced on mDCs in *Nr4a3*⁻/⁻ mice under homeostatic conditions and cannot be increased by TLR-dependent (*C. rodentium* infection) or cytokine-dependent (R848 treatment) activation in vivo.

NR4A3 also regulates the mitochondrial function of DCs during maturation. Pearen and coauthors reported their transcriptomic analysis of muscle-specific *Nr4a3*-trangenic mice and showed that more than 25% of differentially regulated genes were mitochondrial genes (42). This would be consistent with the data of Everts and coauthors, who showed that blocking glycolysis inhibits TLR-dependent DC activation and CCR7 expression (43). Thus, we hypothesized that *Nr4a3* plays a role as a metabolic regulator of DC maturation and activation.

To compare bioenergetic functions of WT and *Nr4a3*⁻/⁻ DCs, we used the Seahorse XFᵉ analyzer to perform a modification of the Mito Stress Test that probes different metabolic states of mitochondria using sequential additions of the ATP synthase inhibitor oligomycin, carbonilcyanide *p*-trifluoromethoxyphenylhydrazone (FCCP) uncoupler, and the respiratory inhibitor antimycin A (44). Both WT and *Nr4a3*⁻/⁻ BMDCs were found to possess some spare respiratory capacity (Figure 6A). This means that these cells are capable of meeting their basic energy demands and compensate for a moderate increase under stress conditions. The observed lower level of basal respiration shown by *Nr4a3*⁻/⁻ BMDCs compared with that of the WT BMDCs is most likely due to a downregulated energy demand of the cells rather than a deficiency in the

number of mitochondria. The above-mentioned preservation of the spare respiratory capacity, maintenance of normal ATP levels (Supplemental Figure 14), and lack of compensatory increase (in fact, a decrease) in the extracellular acid production rate (ECAR) (Figure 6B) all point to this conclusion. However, the maximal respiratory capacity of *Nr4a3*⁻/⁻ BMDCs (induced by FCCP) is approximately one-third lower than that of WT cells.

Oxidative phosphorylation inevitably accompanies ROS production (45), and GM-CSF highly increases ROS production in BMDCs (46). We asked whether the lower basal respiratory capacity of *Nr4a3*⁻/⁻ BMDCs is due to a smaller quantity of mitochondria or to a mitochondrial functional defect. We measured mitochondrial content and ROS production of CD11c⁺ BMDCs with MitoTracker and 2′,7′-dichlorofluorescin diacetate (DCFDA), respectively (Figure 7A). Although mitochondrial content was not different between WT and *Nr4a3*⁻/⁻ BMDCs, ROS production was significantly lower in *Nr4a3*⁻/⁻ BMDCs (Figure 7B). Our data suggest that the observed lower level of basal respiration is probably due to suboptimal mitochondrial function in *Nr4a3*⁻/⁻ BMDCs, but not to the cellular quantity of mitochondria. Thus, our data indicate that NR4A3 also plays a role in maintaining homeostatic mitochondrial function in DCs. Therefore, in addition to being important for the regulation of CCR7 expression, NR4A3 also appears to aid in maintaining adequate cellular respiration of mDCs. However, whether this role for NR4A3 in maintaining cellular respiration has any direct impact on CCR7 expression in this cell type is unclear.

Discussion

The *Nr4a* nuclear receptor family consists of 3 highly homologous proteins that can be simultaneously induced by similar stimuli. However, their expression pattern is both tissue and cell-type specific, indicating that some of their functions are nonredundant. Each *Nr4a* family member has its own specific, nonredundant function. For example, *Nr4a1* plays a selective role in monocyte development (47) that cannot be compensated by *Nr4a2* or *Nr4a3*. However, FOXP3⁺ Treg development is complemented by other family members, and only through deletion of *Nr4a1, Nr4a2,* and *Nr4a3* together is FOXP3⁺ T cell development ablated in vivo (48). Here, we show that CD103⁺ mDCs express higher levels of *Nr4a3* than
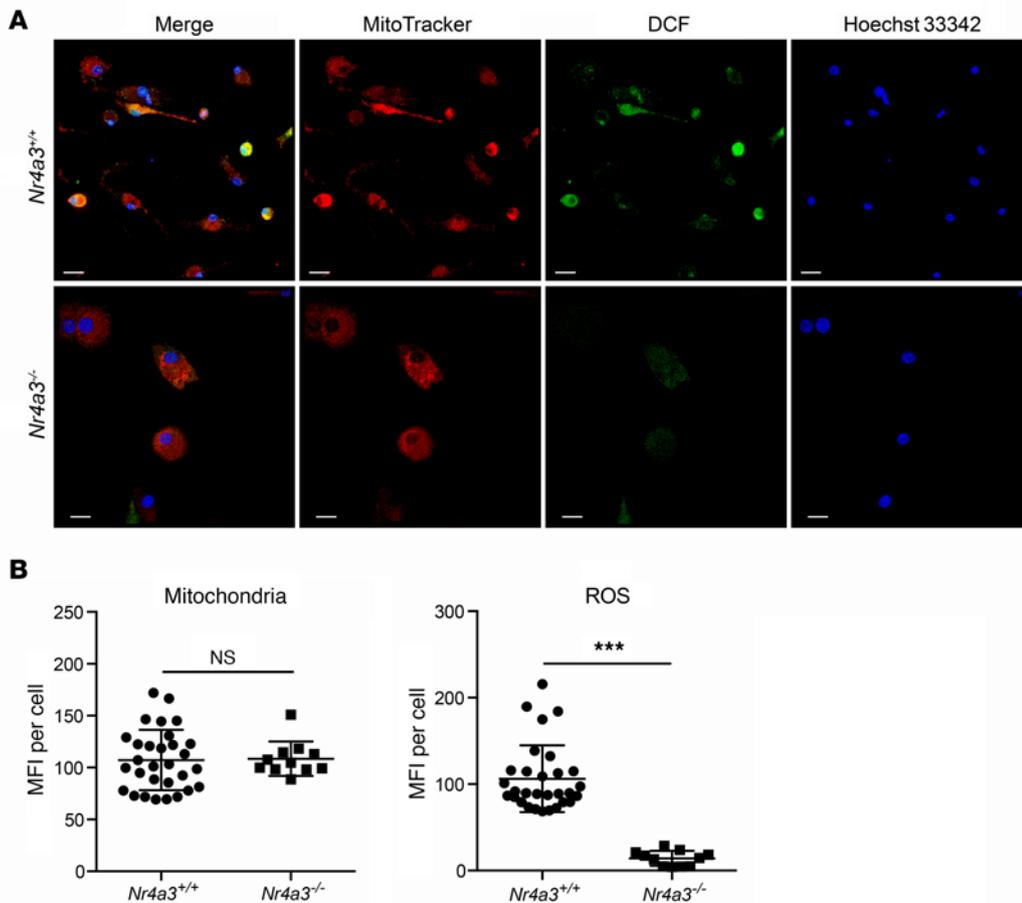
Figure 7. ROS production is lower in day-8 BMDCs from *Nr4a3*^{-/-} mice. (**A**) CD11c⁺ BMDCs were stained with MitoTracker Red CMXRos for mitochondria, DCFDA for ROS, and anti–DC-SIGN for the surface of BMDC and Hoechst 33342 for nuclei. Scale bars: 20 μM. (**B**) DC-SIGN⁺ cells were plotted for fluorescence intensity of MitoTracker and dichlorodihydrofluorescein diacetate (DCFDA). Each dot on the plots represents a single cell. ***$P < 0.0001$, by unpaired, 2-tailed Student's *t* test. Results are representative of 2 independent experiments.

either *Nr4a1* or *Nr4a2* and that the migratory capability of CD103⁺ DCs is uniquely lost in the absence of *Nr4a3*.

In the current study, we show that *Nr4a3* expression in CD103⁺ mDCs is critical for regulating the migratory function of DCs from tissues to LNs in vivo. *Nr4a3* expression is selectively high in the CD103⁺ mDC subset compared with other DC populations, including classical CD11c^{hi} DCs. In the absence of *Nr4a3*, there are markedly reduced numbers of CD103⁺ mDCs in the LNs. Interestingly, CD103⁺ DC numbers in tissues are relatively normal, indicating that *Nr4a3* is not critical for the development of these cells from the precursors present in BM or blood.

CCR7 is required for the migration to LNs of lymphocytes, including T cells (49–51). CCR7 is also quite important for lymphocyte development in the thymus (52, 53). We found that the reduced levels of CCR7 expression in *Nr4a3*^{-/-} mice appeared to be confined to the mDC population, because we observed no differences in CCR7 expression on LN T cells (Figure 4E) or B cells or on developing T cells in the thymus (data not shown). The migratory CD103⁺ mDC subset contained much higher expression levels of *Nr4a3* compared with levels in B or T cells, suggesting that *Nr4a3* plays a major functional role in this DC subset, and perhaps not much of one in T or B cells.

Although *Nr4a3*^{-/-} mice have systemic mDC defects, we and others did not observe any major health problems, except spinning behavior due to an inner ear defect (54). We investigated gut pathology in the small intestine, cecum, and colon of these mice at approximately 8 to 12 weeks of age and found no evidence of colitis

(data not shown). This might be partly due to the fact that the CCR7 defect is specific to DCs and not to T cells. Also, 12 weeks may not be enough time to show inflammatory disease phenotypes based on a DC migratory defect.

DCs mature through both TLR-independent and -dependent pathways, yet both maturation pathways involve the induction of CCR7 expression. To test whether the regulation of DC maturation by NR4A3 occurs through a TLR-dependent or -independent pathway, we performed a series of experiments to test the induction of CCR7 by these pathways both in vitro and in vivo. We found that neither pathway induced CCR7 expression or DC maturation in *Nr4a3*^{-/-} mice. Further, our data suggest that not only CD103⁺ mDCs, but also monocyte-derived inflammatory DCs from *Nr4a3*^{-/-} mice are unable to migrate to LNs in response to external inflammatory stimuli such as *C. rodentium*. Thus, CCR7 cannot be induced by several known activation pathways in *Nr4a3*-deficient mDCs, indicating that *Nr4a3* is definitely required for CCR7 induction in CD103⁺ mDCs.

Interestingly, we found that a likely mechanism for defective CCR7 expression in *Nr4a3*^{-/-} DCs is the posttranscriptional degradation of FOXO1 protein. FOXO1 has been shown to be critical for the regulation of CCR7 activity in DCs through its direct binding to the *Ccr7* promoter (10). Phosphorylation by activated AKT excludes FOXO1 from the nucleus and targets it for polyubiquitination for proteasomal degradation. FOXO1 protein was decreased in *Nr4a3*^{-/-} BMDCs, despite a slight increase in mRNA expression upon LPS stimulation of DCs. Concomitant with this, we observed

an increase in phosphorylated AKT (p-AKT), both at baseline and especially after LPS stimulation. We speculate that NR4A3 regulates AKT phosphorylation in mDCs to prevent the proteasomal degradation of FOXO1, thereby controlling CCR7 expression and influencing the migratory capacity of CD103^{+} DCs. Alternatively, NR4A3 could possibly directly interact with FOXO1 to inhibit its degradation. Briand et al. (55) have shown that NR4A1, an NR4A family member, physically and directly binds to FOXO1 in pancreatic β cells to repress FOXO1 action on insulin secretion, suggesting that NR4A3 may also be able to interact with FOXO1.

Moreover, we observed that *Nr4a3*-deficient mice are more susceptible to death from *C. rodentium*. We anticipate that the sole loss of mDC function does not fully explain the susceptibility of *Nr4a3*^{−/−} mice to *C. rodentium* infection, because *Ccr7*^{−/−} mice are resistant to *C. rodentium* infection, even though they also have no mDCs present in MLNs (56). As such, the susceptibility of *Nr4a3*^{−/−} mice to *C. rodentium* infection suggests additional defective innate immune functions of LPDCs and MLN DCs in *Nr4a3*^{−/−} mice. It is likely, on the basis of these data, that fully functional gut-resident DCs may be crucial for resistance to *C. rodentium* infection in vivo.

The defect in mDC numbers in MLNs in the mixed BM chimeras (Figure 2B) was slightly less severe than that observed in both the global *Nr4a3*-KO and full chimeric mice (Figure 2A). We believe that this is probably due to the following scenario: CCR7 responds to 2 chemokines — CCL21, which is present on lymphatics, and CCL19, which is produced by the mDCs. In the case of the mixed chimera, the presence of WT DCs will generate some CCL19 that can be recognized by CCR7, although the expression of CCR7 on NR4A3-deficient mDCs is very low. In the case of the *Nr4a3*^{−/−} mouse, there is no CCL19 produced at all due to the absence of mDCs, so the phenotype may be more severe. Alternatively, it is quite likely that NR4A3 has additional extrinsic effects that influence the migration of DCs to LNs.

When pre-cDCs extravasate to tissues for terminal differentiation, they face an oxygen gradient from the blood vessel. Hypoxia has been shown to enhance both inflammatory and homeostatic DC maturation, including the regulation of CCR7 expression (57) via HIF-1α (58). Resting DCs rely more on oxidative phosphorylation than on glycolysis (59), which reduces energy expenditure and extends the lifespan of cells. However, DCs instantly turn on glycolysis and fatty acid synthesis when they are stimulated by TLR ligands (43). One possibility is that *Nr4a3* functions as an important metabolic switch for CD103^{+} DC maturation and activation in response to hypoxia. Indeed, muscle-specific *Nr4a3*-transgenic mice showed increased expression of genes involved in energy metabolism, including those that regulate mitochondrial function, oxidative phosphorylation, the TCA cycle, and fatty acid metabolism (42). Concordantly, we found that the mitochondrial function (basal and maximal respiratory capacity) of *Nr4a3*^{−/−} BMDCs is decreased compared with that of WT DCs in the basal state. Lower levels of mitochondrial function of *Nr4a3*^{−/−} DCs were also confirmed by microscopy and ROS production. As such, in the absence of NR4A3, CD103^{+} DCs could not migrate in response to TLR ligands, suggesting impaired respiration in the absence of NR4A3. This is supported by studies by Mancino et al., who showed that DCs with impaired respiratory capacity that were cultured under hypoxic conditions and transferred into healthy recipients are

unable to efficiently migrate to LNs (60). Although a link between energy metabolism and CCR7 regulation exists in the literature (57–59), it is not clear from our studies that NR4A3 directly regulates CCR7 through changes in energy metabolism. Rather, we anticipate that the regulation of CCR7 by NR4A3 is independent of the effect of NR4A3 on mitochondrial respiration. Thus, NR4A3 appears to control genes that happen to impact both mitochondrial respiration and the FOXO1-mediated regulation of CCR7. Both mitochondrial respiration and the FOXO1/CCR7 pathways clearly function to influence CD103^{+} DC migration, and both are regulated by NR4A3 but are probably independent of each other.

In summary, the transcription factor NR4A3 plays a critical role in CD103^{+} DC migration to LNs. Mice lacking *Nr4a3* have reduced numbers of mDCs in lymphatics and LNs. *Nr4a3* is highly expressed in mDCs and indirectly regulates CCR7 expression through FOXO1. In the absence of *Nr4a3*, mDCs are unable to increase CCR7 expression, either through TLR-dependent or -independent pathways, leading to impaired immune responses and survival against pathogens.

Methods

Mice. *Nr4a3*^{−/−} and littermate WT *Nr4a3*^{+/+} mice were gifts of Dennis Bruemmer (University of Pittsburgh, Pittsburgh, Pennsylvania, USA) and Orla Conneely (Baylor College of Medicine, Houston, Texas, USA) and were originally generated and described by Orla Conneely (54). CD11c[YFP] mice [B6.Cg-Tg(Itgax-Venus)1Mnz/J, stock 008829] and congenic CD45.1 (B6.SJL-*Ptprc*[a] *Pep3*[b]/BoyJ, stock 002014) mice were purchased from The Jackson Laboratory. CD11c[YFP] *Nr4a3*^{+/+} and CD11c[YFP] *Nr4a3*^{−/−} mice were generated by crossing CD11c[YFP] mice with *Nr4a3*^{−/−} mice. All mice were fed a standard chow diet containing 0% cholesterol and 5% calories from fat (PicoLab diet 5053; LabDiet). All mice were bred and housed in microisolator cages in a pathogen-free animal facility at the La Jolla Institute for Allergy and Immunology.

Flow cytometry. The following antibodies were used in the experiments: CD103 (clone 2E7, BioLegend); CCR7 (clone 4B12, BioLegend); CD64 (clone X54-5/7.1, BioLegend); CD24 (clone M1/69, BD); CD25 (clone 7D4, BD); I-A/I-E (clone M5/114.15.2, BioLegend); CD45.1 (clone A20, BD); PDCA1 (clone 927, BioLegend); CD45 (clone 30-F11, BioLegend); CD8α (clone 53-6.7, BioLegend); CD3 (clone 145-2C11, BioLegend); CD19 (clone 6D5, Life Technologies); CD11c (clone N418, BioLegend); CD11b (clone M1/70, BD); CD45.2 (clone 104, BioLegend); FOXP3 (clone FJK-16S, eBioscience); CCR9 (clone CW-1.2, eBioscience); TCR-β (clone H57-597, BioLegend); CD4 (clone RM4-5, BioLegend); Thy1.2 (clone 53-2.1, BioLegend); IL-17A (clone eBio17B7, eBioscience); and IFN-γ (clone XMG1.2, BD).

For flow cytometric analysis, cells were incubated with 1 to 2 μg anti-mouse CD16/CD32 (BD) and LIVE/DEAD Fixable Yellow (Life Technologies, Thermo Fisher Scientific) for 15 minutes at 4°C, and the antibody mixture was added and incubated for 30 minutes at 4°C. Tregs were stained with a FOXP3 staining kit (eBioscience). For intracellular cytokine staining, cells were stimulated with 50 ng/ml PMA and 500 ng/ml ionomycin for 4 hours in the presence of GolgiPlug (BD). After surface marker staining, cells were fixed and permeabilized with Cytofix/Cytoperm Fixation/Permeabilization (BD) for cytokine staining. Data were collected using an LSR II Flow Cytometer (BD) and analyzed with FlowJo 9.8 software.

Quantitative RT-PCR. Taqman assays of *Nr4a1, Nr4a2, Nr4a3, Ccr7*, and *Hprt* were purchased from Applied Biosystems (Life Technologies, Thermo Fisher Scientific). Total RNA was isolated using the TRIzol method (Life Technologies, Thermo Fisher Scientific) and/ or an RNeasy Mini Kit (QIAGEN). cDNA was synthesized by using the SuperScript II Reverse Transcriptase System (Life Technologies, Thermo Fisher Scientific). Gene expression reactions were performed using the Taqman Universal Assay Reagent (Applied Biosystems) and a My-iQ II instrument (Bio-Rad). The housekeeping gene *Hprt* was used to normalize the data.

Tissue digestion for intestine, LNs, and spleen. Small intestine (duodenum, jejunum, and ilium) and colon were excised. Food matter and feces were removed, washed with HBSS containing 5% FBS, and mesentery tissue, fat tissue, and Peyer's patches were carefully removed. The small intestine and colon were opened by longitudinal excision. After washing with HBSS containing 5% FBS, the gut tissues were cut into 1-inch-long pieces. The gut tissues were incubated with 25 ml HBSS containing 5% FBS, 5 mM EDTA, 1 mM DTT, and 25 mM HEPES for 15 minutes at 37°C with shaking at 200 rpm. Epithelial cells and intraepithelial lymphocytes were removed, and the remaining tissue was washed 3 times with HBSS containing 5% FBS and 25 mM HEPES. The gut tissue was digested with 25 ml RPMI containing 5% FBS, 25 mM HEPES, 1 mg/ml collagenase D (Roche), and 50 μg/ml DNase I (Roche) for 40 minutes at 37°C with shaking at 200 rpm. After passing through a 100-μm cell strainer, cells were washed with HBSS containing 5% FBS and 25 mM HEPES. Next, cells were isolated by 80% and 40% Percoll (GE Healthcare) gradient centrifugation at 900 *g* for 20 minutes at room temperature, without a break. Interface cells were isolated, washed, and counted with a Vi-CELL counter (Beckman Coulter).

LNs and spleens were excised and chopped after removing the fat tissue. Chopped tissues were digested with RPMI containing 5% FBS, 25 mM HEPES, 1 mg/ml collagenase VIII (Sigma-Aldrich), and 50 μg/ml DNase I (Roche) for 30 minutes at 37°C, with occasional shaking. Cells were passed through a 70-μm cell strainer and washed with PBS containing 2% FBS. Splenic cells were treated with RBC Lysis Buffer (BioLegend) to remove rbc and washed with PBS containing 2% FBS. Total cell numbers were counted with a Coulter Z2 (Beckman Coulter) or a Vi-CELL Counter.

BM stem cell progenitor cell transfer. Stem cell progenitor cells from BM were isolated from CD45.2 *Nr4a3*^{+/+}, CD45.2 *Nr4a3*^{–/–}, and CD45.1 mice using a Mouse Hematopoietic Cell Isolation Kit (STEMCELL Technologies). Briefly, biotinylated antibodies against nonhematopoietic stem and progenitor cells (CD5, CD11b, CD19, CD45R, 7-4, Ly-6G/C [Gr-1], and TER119) were used to remove lineage-positive cells from total BM cells. Enriched lineage-negative cells were used as stem cell progenitor cells. A 1:1 mixture of CD45.1 and CD45.2 stem cell progenitor cells was adoptively transferred into sublethally irradiated (2.75 Gy) CD45.1/2 heterozygous mice via the retro-orbital route. After 10 days, reconstitution of CD45.1 and CD45.2 in blood, colon, and LNs was analyzed by flow cytometry.

Confocal microscopy. CD11c[YFP] *Nr4a3*^{+/+} and CD11c[YFP] *Nr4a3*^{–/–} mice were fed with 10 μg R848 and sacrificed 2 hours later. Mesentery tissue was collected and fixed with 4% paraformaldehyde for 16 hours. After washing out fixatives, the tissues were incubated with PBS containing 2% saponin, 2% FBS, and 0.1% sodium azide for at least 18 hours, as described by Chodaczek et al. (61). Then, the tissues were stained with phycoerythrin-conjugated (PE-conjugated) anti–MHC

II (BD Biosciences) and eFlour 660–conjugated anti–Lyve-1 antibody (1:100; eBioscience) for 18 hours. After washing, the samples were mounted in Prolong Gold Antifade Reagent (Life Technologies, Thermo Fisher Scientific) with a number 1.5 borosilicate glass coverslip. An SP5 resonant laser-scanning confocal system mounted on a DM 6000 upright microscope (Leica Microsystems) with a ×25 water-immersion objective (numerical aperture, 0.95) was used for fluorescence microscopy. Image acquisition was done at room temperature using Leica Application Suite Advanced Fluorescence software. Images used for 3D reconstructions were acquired with a 2-μm Z-step size and 488-nm and 633-nm excitation wavelengths to visualize yellow fluorescent protein–labeled (YFP-labeled) cells and eFluor 660–labeled lymphatic vessels. Fluorescent signals were detected with internal photomultiplier tubes. Image analysis was done using Imaris 8.12 software (Bitplane). Lyve-1–labeled structures were isosurfaced, and distance transformation was applied to create a new channel that encoded the 3D distance from the lymphatic vessels. CD11c[YFP] cells were isosurfaced and classified as being associated with lymphatics when the distance from the nearest Lyve-1–positive structure was less than 15 μm. To normalize between data sets, the number of cells associated with lymphatics was divided by the volume of lymphatic vessels (expressed in μm³ and divided by 100,000).

For ROS visualization, CD11c^{+} cells were isolated from day-7 BMDC cultures and plated on pre-cleaned 1-mm glass coverslips overnight. The cells were mounted on a microscope slide with HBSS and placed on a heated plate at 33.5°C. To visualize DCs, mitochondria, and oxidative function, all cells were stained with APC-conjugated APC Armenian Hamster Anti-mouse DC-SIGN (1:100; eBioscience); MitoTracker Red CMXRos (200 μm/ml; Thermo Fisher Scientific); and DCFDA (5 μm/ml; Abcam) for 30 minutes at 37°C, respectively. To visualize nuclei, Hoechst 33342 (Thermo Fisher Scientific) was subsequently added at 10 μl/ml for 5 minutes at 37°C. Cells were washed and imaged within the hour. Leica Acquisition Suite Advanced Fluorescence software was used to capture 3 images per slide, with visible lasers at 488-nm, 543-nm, 633-nm excitation wavelengths, an infrared laser tuned to 800 nm, and a 1.8-μm Z-step. Imaris 8 software (Bitplane) was used to mask DC-SIGN^{+} cells and analyze pixel intensity for each channel. The mean intensity for MitoTracker Red and DCFDA for each whole cell was plotted for each experiment.

BMDC culture. BM cells from *Nr4a3*^{+/+} and *Nr4a3*^{–/–} mice were cultured by following a previously described method (62). Briefly, 2 million BM cells were plated onto a 6-well plate with RPMI containing 10% FBS, 20 ng/ml GM-CSF (Peprotech), 2 mM glutamine, 50 μM β-mercaptoethanol, and 1× antibiotic-antimycotic (Gibco, Life Technologies, Thermo Fisher Scientific). Fifty percent of the culture media was changed every other day. Cells cultured between days 7 and 9 were used for experiments.

Ccr7 promoter analysis and transcription factor binding site prediction. 3.3kb upstream DNA sequence from the translation initiation site of the mouse Ccr7 promoter was analyzed by MacVector software (version 12.7.5.). Transcription factor binding sites were predicted with 90% homology setting using JASPAR database. This 3.3kb of the murine Ccr7 promoter sequence was cloned into pGL4 luciferase vector (Promega). cDNA expression clones of Nr4a3 and C/EBP beta genes cloned into pCMV6-Entry vector were purchased from OriGene. Constitutive beta-galactosidase plasmid, pGL4 Ccr7 reporter plasmid and Nr4a3 or C/EBP plasmids were co-transfected into RAW264.7 or

293T cells. After 18 hrs, cells were lysed and a dual reporter assay was performed using a single automatic injection Mithras (Berthold technologies) luminometer following the manufacturer's protocol (Promega). Ratios of Luciferase activity and beta-galactosidase activity were normalized to an empty reporter construct.

Immunoblotting. CD11c^{+} cells isolated from day-8 BMDC cultures were plated at 2 million cells per well and stimulated with or without 0.5 μg/ml LPS for 18 hours. Cells were lysed with RIPA buffer. After total protein was quantified by using a Pierce BCA Protein Assay Kit (Thermo Fisher Scientific), an equal amount of protein was loaded and separated in a 4% to 12% Bis-Tris NuPAGE Precast Gel (Invitrogen, Thermo Fisher Scientific). Protein was transferred to a 0.45-μm nitrocellulose membrane. The membrane was blocked and incubated with the following antibodies: anti-FOXO1, anti-AKT, anti–p-AKT (Ser473), and anti–β-actin (all from Cell Signaling Technology). Primary antibodies were detected by HRP-conjugated anti-rabbit IgG, and blots were developed using SuperSignal West Pico Chemiluminescent Substrate (Thermo Fisher Scientific).

Infection model. $Nr4a3^{-/-}$ and $Nr4a3^{+/+}$ mice were cohoused and maintained on nonacidic water for more than 4 weeks before steady-state and infection experiments. Age- and sex-matched male and female mice were used for all experiments, except for the *C. rodentium* survival experiment, in which 8- to 12-week-old female mice were used. A chloramphenicol-resistant variant of the WT *C. rodentium* strain DBS100 was cultured as previously described (63). $Nr4a3^{+/+}$ and $Nr4a3^{-/-}$ mice were orally infected with 1×10^9 CFU *C. rodentium*. The appearance and survival of infected mice were monitored daily for 21 days. DCs, Th1 cells, and Th17 cells were analyzed 8 days after infection. Bacterial burden was measured by plating feces and splenic and liver tissue.

Energy metabolism of BMDC. Energy metabolism of BMDCs was assessed with an XF^{e}96 Flux Analyzer (Seahorse Bioscience). CD11c^{+} cells were selected from day-8 BMDCs using CD11C microbeads (Miltenyi Biotec). Cells were plated on Seahorse cell culture plates in their growth medium at a density of 10^5 cells per well and then stimulated with LPS for 16 hours prior to the experiment. Immediately before measurement, the medium was removed, and the adherent cells were gently washed with assay buffer (unbuffered DMEM, prepared according to Seahorse Bioscience protocols, supplemented with 10 mM glucose, 10 mM sodium pyruvate, 1× GlutaMax, and 1 mM HEPES, pH 7.4). The wells were filled with 450 μl/well assay buffer, and the measurements were initiated. Oxygen consumption rates (OCRs) and ECARs were normalized by Hoechst 33342 fluorescence from nuclei staining.

Statistics. Data were analyzed with GraphPad Prism 6.0 (GraphPad Software). Statistical significance was calculated by an unpaired, 2-tailed Student's *t* test or 2-way ANOVA. A *P* value of less than 0.05 was considered statistically significant.

Study approval. All experiments followed the guidelines of the IACUC of the La Jolla Institute for Allergy and Immunology. Approval of the use of rodents was obtained from the La Jolla Institute for Allergy and Immunology Animal Care and Use Committee, according to NIH guidelines for the care and use of laboratory animals.

Author contributions

Acknowledgments

Address correspondence to: Catherine C. Hedrick, Division of Inflammation Biology, La Jolla Institute for Allergy and Immunology, 9420 Athena Circle, La Jolla, California 92037, USA. Phone: 858.752.6500; E-mail: hedrick@lji.org.

1. Schulz O, et al. Intestinal CD103+, but not CX3CR1+, antigen sampling cells migrate in lymph and serve classical dendritic cell functions. *J Exp Med*. 2009;206(13):3101–3114.

2. Jang MH, et al. CCR7 is critically important for migration of dendritic cells in intestinal lamina propria to mesenteric lymph nodes. *J Immunol*. 2006;176(2):803–810.

3. Coombes JL, et al. A functionally specialized population of mucosal CD103+ DCs induces Foxp3+ regulatory T cells via a TGF-beta and retinoic acid-dependent mechanism. *J Exp Med*. 2007;204(8):1757–1764.

4. Bogunovic M, et al. Origin of the lamina propria dendritic cell network. *Immunity*. 2009;31(3):513–525.

5. Schreiber HA, et al. Intestinal monocytes and macrophages are required for T cell polarization in response to Citrobacter rodentium. *J Exp Med*. 2013;210(10):2025–2039.

6. Scott CL, Aumeunier AM, Mowat AM. Intestinal CD103+ dendritic cells: master regulators of tolerance? *Trends Immunol*. 2011;32(9):412–419.

7. Welty NE, Staley C, Ghilardi N, Sadowsky MJ, Igyártó BZ, Kaplan DH. Intestinal lamina propria dendritic cells maintain T cell homeostasis but do not affect commensalism. *J Exp Med*. 2013;210(10):2011–2024.

8. Fainaru O, Shseyov D, Hantisteanu S, Groner Y. Accelerated chemokine receptor 7-mediated dendritic cell migration in Runx3 knockout mice and the spontaneous development of asthma-like disease. *Proc Natl Acad Sci U S A*. 2005;102(30):10598–10603.

9. Kerdiles YM, et al. Foxo1 links homing and survival of naive T cells by regulating L-selectin, CCR7 and interleukin 7 receptor. *Nat Immunol*. 2009;10(2):176–184.

10. Dong G, et al. FOXO1 regulates dendritic cell activity through ICAM-1 and CCR7. *J Immunol*. 2015;194(8):3745–3755.

11. Mburu YK, et al. Chemokine receptor 7 (CCR7) gene expression is regulated by NF-κB and activator protein 1 (AP1) in metastatic squamous cell carcinoma of head and neck (SCCHN). *J Biol Chem*. 2012;287(5):3581–3590.

12. Feig JE, et al. LXR promotes the maximal egress of monocyte-derived cells from mouse aortic plaques during atherosclerosis regression. *J Clin Invest*. 2010;120(12):4415–4424.

13. Bruckner M, Dickel D, Singer E, Legler DF. Converse regulation of CCR7-driven human dendritic cell migration by prostaglandin E$_2$ and liver X receptor activation. *Eur J Immunol*. 2012;42(11):2949–2958.

14. Wu C, et al. Modulation of Macrophage Gene Expression via Liver X Receptor α Serine 198 Phosphorylation. *Mol Cell Biol*. 2015;35(11):2024–2034.

15. Côté SC, Pasvanis S, Bounou S, Dumais N. CCR7-specific migration to CCL19 and CCL21 is induced by PGE(2) stimulation in human monocytes: Involvement of EP(2)/EP(4) receptors activation. *Mol Immunol*. 2009;46(13):2682–2693.

16. Legler DF, Krause P, Scandella E, Singer E, Groettrup M. Prostaglandin E2 is generally required for human dendritic cell migration and exerts its effect via EP2 and EP4 receptors. *J Immunol*. 2006;176(2):966–973.

17. Kitajima M, Ziegler SF. Cutting edge: identifica-

tion of the thymic stromal lymphopoietin-responsive dendritic cell subset critical for initiation of type 2 contact hypersensitivity. *J Immunol*. 2013;191(10):4903–4907.

18. Yen JH, Kong W, Ganea D. IFN-beta inhibits dendritic cell migration through STAT-1-mediated transcriptional suppression of CCR7 and matrix metalloproteinase 9. *J Immunol*. 2010;184(7):3478–3486.

19. Maxwell MA, Muscat GE. The NR4A subgroup: immediate early response genes with pleiotropic physiological roles. *Nucl Recept Signal*. 2006;4:e002.

20. Pönniö T, Conneely OM. nor-1 regulates hippocampal axon guidance, pyramidal cell survival, and seizure susceptibility. *Mol Cell Biol*. 2004;24(20):9070–9078.

21. Nomiyama T, et al. The NR4A orphan nuclear receptor NOR1 is induced by platelet-derived growth factor and mediates vascular smooth muscle cell proliferation. *J Biol Chem*. 2006;281(44):33467–33476.

22. Qing H, et al. Deficiency of the NR4A orphan nuclear receptor NOR1 in hematopoietic stem cells accelerates atherosclerosis. *Stem Cells*. 2014;32(9):2419–2429.

23. Cheng LE, Chan FK, Cado D, Winoto A. Functional redundancy of the Nur77 and Nor-1 orphan steroid receptors in T-cell apoptosis. *EMBO J*. 1997;16(8):1865–1875.

24. Pei L, Castrillo A, Chen M, Hoffmann A, Tontonoz P. Induction of NR4A orphan nuclear receptor expression in macrophages in response to inflammatory stimuli. *J Biol Chem*. 2005;280(32):29256–29262.

25. Hanna RN, et al. NR4A1 (Nur77) deletion polarizes macrophages toward an inflammatory phenotype and increases atherosclerosis. *Circ Res*. 2012;110(3):416–427.

26. Wang T, et al. Inhibition of activation-induced death of dendritic cells and enhancement of vaccine efficacy via blockade of MINOR. *Blood*. 2009;113(13):2906–2913.

27. Ng SS, Chang TH, Tailor P, Ozato K, Kino T. Virus-induced differential expression of nuclear receptors and coregulators in dendritic cells: implication to interferon production. *FEBS Lett*. 2011;585(9):1331–1337.

28. Grajales-Reyes GE, et al. Batf3 maintains autoactivation of Irf8 for commitment of a CD8α(+) conventional DC clonogenic progenitor. *Nat Immunol*. 2015;16(7):708–717.

29. Villadangos JA, Schnorrer P. Intrinsic and cooperative antigen-presenting functions of dendritic-cell subsets in vivo. *Nat Rev Immunol*. 2007;7(7):543–555.

30. Ginhoux F, et al. The origin and development of nonlymphoid tissue CD103+ DCs. *J Exp Med*. 2009;206(13):3115–3130.

31. Varol C, et al. Intestinal lamina propria dendritic cell subsets have different origin and functions. *Immunity*. 2009;31(3):502–512.

32. Tamoutounour S, et al. CD64 distinguishes macrophages from dendritic cells in the gut and reveals the Th1-inducing role of mesenteric lymph node macrophages during colitis. *Eur J Immunol*. 2012;42(12):3150–3166.

33. Bain CC, et al. Resident and pro-inflammatory macrophages in the colon represent alternative context-dependent fates of the same Ly6Chi monocyte precursors. *Mucosal Immunol*. 2013;6(3):498–510.

34. Randolph GJ, Angeli V, Swartz MA. Dendritic-cell trafficking to lymph nodes through lymphatic vessels. *Nat Rev Immunol*. 2005;5(8):617–628.

35. Huang H, Tindall DJ. Regulation of FOXO protein stability via ubiquitination and proteasome degradation. *Biochim Biophys Acta*. 2011;1813(11):1961–1964.

36. Johansson-Lindbom B, Svensson M, Wurbel MA, Malissen B, Márquez G, Agace W. Selective generation of gut tropic T cells in gut-associated lymphoid tissue (GALT): requirement for GALT dendritic cells and adjuvant. *J Exp Med*. 2003;198(6):963–969.

37. Iwata M, Hirakiyama A, Eshima Y, Kagechika H, Kato C, Song SY. Retinoic acid imprints gut-homing specificity on T cells. *Immunity*. 2004;21(4):527–538.

38. Yrlid U, Milling SW, Miller JL, Cartland S, Jenkins CD, MacPherson GG. Regulation of intestinal dendritic cell migration and activation by plasmacytoid dendritic cells, TNF-alpha and type 1 IFNs after feeding a TLR7/8 ligand. *J Immunol*. 2006;176(9):5205–5212.

39. Worbs T, et al. Oral tolerance originates in the intestinal immune system and relies on antigen carriage by dendritic cells. *J Exp Med*. 2006;203(3):519–527.

40. Jiang A, et al. Disruption of E-cadherin-mediated adhesion induces a functionally distinct pathway of dendritic cell maturation. *Immunity*. 2007;27(4):610–624.

41. Mundy R, MacDonald TT, Dougan G, Frankel G, Wiles S. Citrobacter rodentium of mice and man. *Cell Microbiol*. 2005;7(12):1697–1706.

42. Pearen MA, et al. Transgenic muscle-specific Nor-1 expression regulates multiple pathways that effect adiposity, metabolism, and endurance. *Mol Endocrinol*. 2013;27(11):1897–1917.

43. Everts B, et al. TLR-driven early glycolytic reprogramming via the kinases TBK1-IKKε supports the anabolic demands of dendritic cell activation. *Nat Immunol*. 2014;15(4):323–332.

44. Andreyev AY, et al. Isotope-reinforced polyunsaturated fatty acids protect mitochondria from oxidative stress. *Free Radic Biol Med*. 2015;82:63–72.

45. Andreyev AY, Kushnareva YE, Murphy AN, Starkov AA. Mitochondrial ROS Metabolism: 10 Years Later. *Biochemistry Mosc*. 2015;80(5):517–531.

46. Del Prete A, et al. Role of mitochondria and reactive oxygen species in dendritic cell differentiation and functions. *Free Radic Biol Med*. 2008;44(7):1443–1451.

47. Hanna RN, et al. The transcription factor NR4A1 (Nur77) controls bone marrow differentiation and the survival of Ly6C- monocytes. *Nat Immunol*. 2011;12(8):778–785.

48. Sekiya T, et al. Nr4a receptors are essential for thymic regulatory T cell development and immune homeostasis. *Nat Immunol*. 2013;14(3):230–237.

49. Bromley SK, Thomas SY, Luster AD. Chemokine receptor CCR7 guides T cell exit from peripheral tissues and entry into afferent lymphatics. *Nat Immunol*. 2005;6(9):895–901.

50. Debes GF, et al. Chemokine receptor CCR7 required for T lymphocyte exit from peripheral tissues. *Nat Immunol*. 2005;6(9):889–894.

51. Badr G, Borhis G, Treton D, Richard Y. IFN {alpha} enhances human B-cell chemotaxis by modulating ligand-induced chemokine receptor signaling and internalization. *Int Immunol*. 2005;17(4):459–467.

52. Comerford I, Harata-Lee Y, Bunting MD, Gregor C, Kara EE, McColl SR. A myriad of functions and complex regulation of the CCR7/CCL19/CCL21 chemokine axis in the adaptive immune system. *Cytokine Growth Factor Rev*. 2013;24(3):269–283.

53. Förster R, Davalos-Misslitz AC, Rot A. CCR7 and its ligands: balancing immunity and tolerance. *Nat Rev Immunol*. 2008;8(5):362–371.

54. Ponnio T, Burton Q, Pereira FA, Wu DK, Conneely OM. The nuclear receptor Nor-1 is essential for proliferation of the semicircular canals of the mouse inner ear. *Mol Cell Biol*. 2002;22(3):935–945.

55. Briand O, et al. The nuclear orphan receptor Nur77 is a lipotoxicity sensor regulating glucose-induced insulin secretion in pancreatic β-cells. *Mol Endocrinol*. 2012;26(3):399–413.

56. Satpathy AT, et al. Notch2-dependent classical dendritic cells orchestrate intestinal immunity to attaching-and-effacing bacterial pathogens. *Nat Immunol*. 2013;14(9):937–948.

57. Bosco MC, et al. Monocytes and dendritic cells in a hypoxic environment: Spotlights on chemotaxis and migration. *Immunobiology*. 2008;213(9-10):733–749.

58. Köhler T, Reizis B, Johnson RS, Weighardt H, Förster I. Influence of hypoxia-inducible factor 1α on dendritic cell differentiation and migration. *Eur J Immunol*. 2012;42(5):1226–1236.

59. Krawczyk CM, et al. Toll-like receptor-induced changes in glycolytic metabolism regulate dendritic cell activation. *Blood*. 2010;115(23):4742–4749.

60. Mancino A, et al. Divergent effects of hypoxia on dendritic cell functions. *Blood*. 2008;112(9):3723–3734.

61. Chodaczek G, Papanna V, Zal MA, Zal T. Body-barrier surveillance by epidermal γδ TCRs. *Nat Immunol*. 2012;13(3):272–282.

62. Lutz MB, et al. An advanced culture method for generating large quantities of highly pure dendritic cells from mouse bone marrow. *J Immunol Methods*. 1999;223(1):77–92.

63. Shui JW, et al. HVEM signalling at mucosal barriers provides host defence against pathogenic bacteria. *Nature*. 2012;488(7410):222–225.